DATA PAPER

Optical spectroscopy of CrO and electronic states of the Cr group metal monoxides

Lei Zhang(张磊)[1,2], Yao Yu(于尧)[1,2], Xinwen Ma(马新文)[1,3,4], and Jie Yang(杨杰)[1,3,4,†]

[1] *Institute of Modern Physics, Chinese Academy of Sciences, Lanzhou* 730000, *China*
[2] *University of Chinese Academy of Sciences, Beijing* 100049, *China*
[3] *Advanced Energy Science and Technology Guangdong Laboratory, Huizhou* 516003, *China*
[4] *CAS Key Laboratory of High Precision Nuclear Spectroscopy, Institute of Modern Physics, Chinese Academy of Sciences, Lanzhou* 73000, *China*

(Received 9 November 2022; revised manuscript received 29 January 2023; accepted manuscript online 31 January 2023)

All of the experimentally known electronic states of the Cr group metal monoxides (CrO, MoO, and WO) have been presented in the paper. The optical spectra of the CrO molecule have been investigated in the gas phase through a combination of the laser-induced fluorescence (LIF) excitation and single-vibronic-level (SVL) emission spectroscopy in the supersonic expansion. The rotational constants of the vibronic electronic states, including $X\,^5\Pi_{-1}$ ($v'' = 0$–3), $B\,^5\Pi_{-1}$ ($v' = 0$–10), and $B\,^5\Pi_1$ ($v' = 1$, 5), and the vibrational constants of the spin–orbit components $X\,^5\Pi_{-1,0,1}$ have been obtained. The molecular constants of the MoO and WO molecules have been summarized by reviewing the previous spectroscopic studies, and a comprehensive energy level diagram of the Cr group metal monoxides has been constructed. By comparing the electronic configurations, bond lengths, and vibrational frequencies of all the transition metal monoxides in the ground electronic state, the significance of the relativistic effect in the bonding of the 5d transition metal monoxides has been discussed. The related spectroscopic data of the CrO molecule are available at https://doi.org/10.57760/sciencedb.j00113.00085.

Keywords: laser-induced fluorescence (LIF), transition metal monoxide, electronic state, molecular constant, relativistic effect

PACS: 33.20.Kf, 33.20.Vq, 33.15.Mt, 36.20.Kd **DOI:** 10.1088/1674-1056/acb763

1. Introduction

The accurate description of the electronic states of the transition metal monoxides is of fundamental importance for optimizing the computational methods and programs in modern quantum chemistry,[1–3] characterizing the properties of the bonding between metal and oxide,[4–7] and probing stellar compositions and evolution.[8–11] The open atomic d-shell of the transition metal atoms would result in many molecular low-lying electronic states with high spin multiplicity.[12,13] Moreover, the large spin–orbit splitting and strong relativistic effect in the 5d transition metal atoms may cause the electronic states of the molecules more complex. These give rise to that the analyses and understanding of the electronic structures of the transition metal monoxides become a challenge to both experimenters and theorists.

For the Cr group transition metals (Cr, Mo, and W), the monoxides are representative of both the s and d electrons bondings due to the features on the half-filled nd$(n+1)$s atomic valence shell. The electronic structures of CrO,[14–27] MoO,[27–36] and WO[37–50] have been studied for a long time by the optical spectroscopy and theoretical computation. Up to recent years, there were still many spectroscopic reports on MoO and WO, especially the measurement on the spin–orbit splitting of the ground electronic state.[35,51] For CrO, the latest experiment of the optical spectroscopy was reported two decades ago,[25] and the knowledge about the excited states was limited in a narrow energy range from near-infra to orange.

The optical spectra of CrO are experimentally the earliest recorded among the Cr group metal monoxides, because its first observation can go back to 1911.[14] CrO is one of the most important molecules in astrophysics since it was identified in the spectra of the star β Pegasi in 1947,[8] and recently identified in the astronomical spectrum of V1309 Sco.[9] In 1932, Ferguson[15] reported a very strong electronic transition system of CrO in the orange-red region. In 1955, this system was assigned as $^5\Pi$–$^5\Pi$ from a rotational analysis by Ninomiya.[16] In 1980, the (2-0), (1-0), (0-0), (0-1), and (0-2) bands of $B\,^5\Pi$–$X\,^5\Pi$ were presented by a more complete rotational analysis by Hocking *et al.*[18] In 1984, the rotationally resolved $A\,^5\Sigma$–$X\,^5\Pi$ (0-0) band (near 8000 cm^{-1}) was newly observed by Cheung *et al.*,[19] and the spin–orbit splitting of the ground electronic state was determined. And then two theoretical works presented by Bauschlicher[26] and Nelin *et al.*[27] in 1985 suggested that the A state ought to be assigned as $^5\Sigma^+$. In 1993, Barnes *et al.*[20] observed the (0-0) and (1-1) bands of the $A'\,^5\Delta$–$X\,^5\Pi$ transition (near 11800 cm^{-1}) with rotational resolution. In addition, three triplet states, including $^3\Sigma^+$, $^3\Pi$, and $^3\Phi$, were presented in two photoelectron

†Corresponding author. E-mail: jie.yang@impcas.ac.cn

© 2023 Chinese Physical Society and IOP Publishing Ltd

spectroscopy experiments, which were reported by Wenthold *et al.*[21] in 1996 and Gutsev *et al.*[24] in 2001. In 2002, Sheridan *et al.*[25] characterized the ground electronic state of CrO through the pure rotational spectra.

In this paper, using the laser ablation technique combining with the supersonic free jet expansion, the laser induced fluorescence (LIF) excitation spectra and single-vibronic-level (SVL) emission spectra of CrO have been observed in the energy range of 13800–23200 cm^{-1}, and the molecular constants in the X and B states have been obtained. To understand the properties of the electronic structures of the Cr group metal monoxides, a collection of the molecular constants of MoO and WO has been provided. In addition, the relativistic effect in the bonding of the 5d transition metal monoxides has been discussed by comparing the electronic configurations, bond lengths and vibrational frequencies of all the transition metal monoxides in the ground electronic states.

The paper is structured as follows: the experimental setup and the analysis method are introduced in Section 2. The observed optical spectra of CrO are presented and analyzed, and the experimentally known electronic states of MoO and WO are reviewed in Section 3. The discussions about the electronic configurations of the Cr group metal monoxides and the relativistic effect in the 5d transition metal monoxides are presented in Section 4. At last, a summary is the content of Section 5.

2. Experimental schemes and spectroscopic analysis

2.1. Experimental setup

In this work, we have observed the LIF excitation and SVL emission spectra of the CrO molecule in the gas phase. The schematic diagram of the experimental setup is shown in Fig. 1. This setup mainly consists of the jet-cooled molecular generation system (including the target of pure metal or metal compound, discharge electrode, carrier gas, pulsed valve, and vacuum chamber), the laser system (including the ablation laser, pump laser, and molecular excitation laser), and the signal acquisition system (including the delay generator, detectors, monochromator, signal converter, and computer).

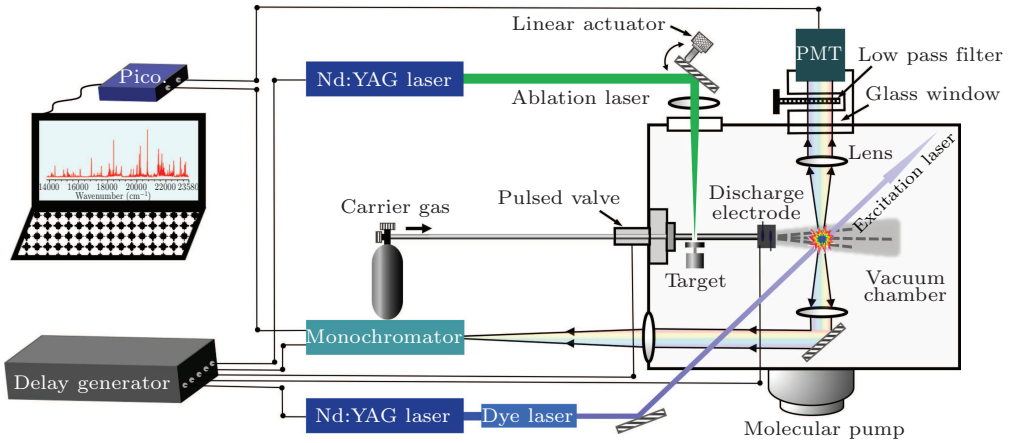


Fig. 1. Schematic diagram of the experimental setup.

In the experiment, the gas-phase CrO molecule was produced by a Nd:YAG laser (Beamtech, SGR-10, 532 nm, 10 Hz) ablating a bulk chromium oxide (Cr_2O_3) target. In order to provide a stable molecular source, the ablation laser was kept at a stable power (about 15 mJ/pulse before focusing), and the target was rotated to prevent the surface from being drilled. The CrO molecules were carried by the argon supersonic molecular beam produced by a pulsed valve (General Valve 99, nozzle diameter 0.5 mm, pulse width 260 μs, 10 Hz, stagnation pressure 120 Psi). With supersonic cooling, the rotational temperature of the CrO molecule was cooled to 40 K downstream 5 cm from the ablation region.

In the excitation area, a tunable pulsed dye laser (Sirah, Cobra-Stretch, linewidth 0.02 cm^{-1}, output 415–725 nm, 0.1 mJ/pulse) pumped by the third harmonic of a Nd:YAG laser (Continuum, Surelite II-10, 10 Hz) crossed perpendicularly with the jet flow. The wavelength of the excitation laser was calibrated to an accuracy of 0.02 cm^{-1} by a wavelength meter (HighFinesse, WS7-60), which has an absolute accuracy of 200 MHz under the pulsed mode. The spectrum of I_2 was used as a standard reference to check the accuracy, repeatability, and stability of the dye laser and wavelength meter. In daily use, the wavelength meter is calibrated by the saturated absorption spectrum of rubidium atoms to an accuracy of 10 MHz in the continue laser mode every three months in our laboratory.[52] The fluorescence decaying from the excited states was collected by two lens systems. Part of the fluorescence was guided into a photomultiplier tube (PMT, EMI, ET9202QB) detector by the top lens system through a suitable low pass filter. The LIF excitation spectra were recorded by

the PMT detector monitoring the fluorescence intensity with the wavelength changes of the excitation laser. The bottom lens system focused part of the fluorescence into a monochromator (HORIBA, JY1000M-II, focal length 1 m, nominal dispersion 0.8 nm/mm, equipped with an 1800 lines/mm grating blazed at 750 nm). The dispersed fluorescence was detected by a thermoelectrically cooled PMT (Hamamatsu, R928) detector, and provided the SVL emission spectra when the excitation laser was fixed at a certain position. The accuracy of the monochromator was calibrated by the emission spectrum of argon (covering 11500–24000 cm^{-1}) to 1 cm^{-1}.

The appropriate relative time delays among the ablation laser, excitation laser, and pulsed valve were controlled by a pulsed multichannel delay generator (Quantum 9400, 8 channels). A digital oscilloscope card (Pico5444B, 4 channels, sampling rate 1 GHz) was used to convert the analog signals obtained from the two PMT detectors to the digital signals. A home-made program based on LabVIEW software was used to communicate with the dye laser and monochromator and to save the data on a personal computer.

2.2. Rovibronic analysis

For a diatomic molecule, the vibrational progression can be expressed under an anharmonic oscillator model as the formula[53]

$$T(v) = T_e + \omega_e(v+1/2) - \omega_e x_e(v+1/2)^2 + \omega_e y_e(v+1/2)^3. \quad (1)$$

In vibrational analysis, the least-square method is used to fit the observed vibrational levels to obtain the electronic state term energy T_e, vibrational frequency ω_e, and vibrational anharmonicity constants, $\omega_e x_e$ and $\omega_e y_e$.

The rotational energy of a diatomic molecule is considered as[53]

$$F(J) = T_{veff} + B_v J(J+1) - D_v[J(J+1)]^2 \pm qJ(J+1)/2 \quad (2)$$

in Hund's case (a) coupling scheme when the spin quantum number is zero, in which J is the rotational quantum number; T_{veff} is the effective term energy; q is the Λ-doubling parameter; B_v and D_v are the rotational constant and centrifugal distortion constant, respectively. When the spin quantum number is not zero, it is necessary to consider all the spin–orbit components to accurately determine the rotational levels of the electronic state. However, Eq. (2) is approximately applicable for describing the energy of the rotational level with small J value.

The rotational constant B_v is associated with the vibrational energy level v and the equilibrium rotational constant B_e[53]

$$B_v = B_e - \alpha_e(v+1/2) + \gamma_e(v+1/2)^2. \quad (3)$$

Here α_e and γ_e are the higher order equilibrium rotational constants, which are much smaller compared to B_e. In addition, the bond length r can be derived from the rotational constant based on the formula $r = [h/(8\pi^2\mu B)]^{1/2}$,[53] where μ is the reduced mass in units of amu.

The PGOPHER software[55] is employed to analyze the rotationally resolved LIF excitation spectra, in which an appropriate effective Hamiltonian is chosen as $\boldsymbol{H} = \boldsymbol{H}_{rot} + \boldsymbol{H}_{cd} + \boldsymbol{H}_{LD}$, and the three terms represent the rotational kinetic energy, centrifugal distortion energy, and Λ-doubling coupling, respectively. By fitting the rotationally resolved spectra through PGOPHER, the rotational constants in the lower and upper states are obtained.

3. Spectroscopic information on CrO, MoO, and WO

3.1. LIF excitation spectra of CrO

Figure 2 displays an overall LIF excitation spectrum of CrO in the energy range of 13800–23200 cm^{-1} with low-resolution (0.1 cm^{-1}). In this region, 35 vibronic bands are identified to the $^{52}Cr^{16}O$ isotopologue, since the natural abundance of ^{52}Cr (83.789%) is much larger than that of ^{53}Cr (9.501%), ^{50}Cr (4.345%) and ^{54}Cr (2.365%).[56] The observed bands are assigned to three transitions, i.e., $B\,^5\Pi_{-1,0,1}$–$X\,^5\Pi_{-1}$. Prior to this work, the rotationally resolved (0-2), (0-1), (0-0), (1-0), and (2-0) bands of B $^5\Pi$–$X\,^5\Pi$ have been reported in Ref. [19]. In this work, 16 vibronic bands are rotationally resolved within a typical resolution of 0.04 cm^{-1}, including the (v'-0) with $v' = 0$–10, (0-1), (1-2), and (3-3) bands of $B\,^5\Pi_{-1}$–$X\,^5\Pi_{-1}$ and the (1-0) and (5-0) bands of $B\,^5\Pi_1$–$X\,^5\Pi_{-1}$. All the rotationally resolved bands and the corresponding fitting results are provided in supplementary material. These bands are identified with small J'' (≤ 16) values, and Eq. (2) is therefore adequate to describe the rotational structure, although the complete spin–orbit components have not fully observed. For the (0-0) and (1-0) bands of $B\,^5\Pi_0$–$X\,^5\Pi_{-1}$ and the (0-0) band of $B\,^5\Pi_1$–$X\,^5\Pi_{-1}$, the spectra are too complicated to be analyzed due to the irregular Λ-doubling and possible perturbation in the upper states. In Fig. 2, it should be noted that the relative intensities of different vibronic bands are not completely credible because the spectrum is a composite of more than one laser dye scan with the variable laser power. In the experiment, only the $X\,^5\Pi_{-1}$ component was identified in the ground electronic state, which is attributed to the higher Ω-components being hard to thermally populate in the supersonic beam with the rotational temperature of about 40 K. Although some additional lines observed in some rotationally resolved spectra may be the excitations of other ground Ω-components, these transitions are too weak to be identified accurately.

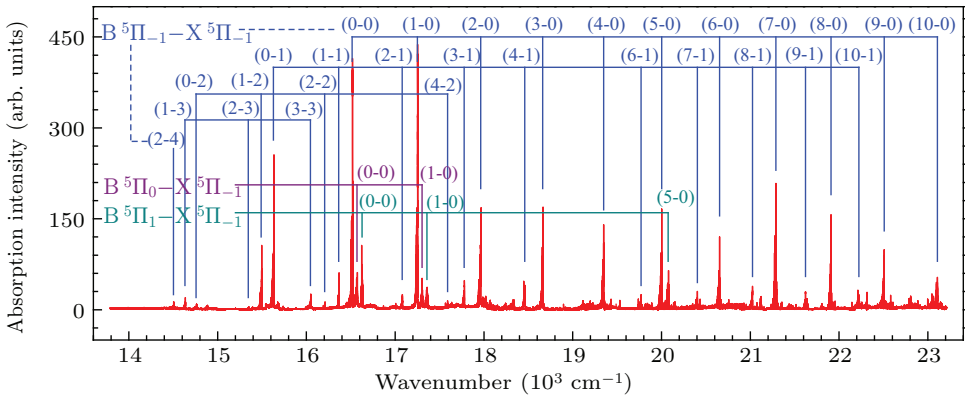


Fig. 2. Low-resolution LIF excitation spectrum of CrO within 13800–23200 cm^{-1}. 34 vibronic bands are assigned to the B $^5\Pi$–X $^5\Pi$ transition and labeled by ticks.

A. The B $^5\Pi_{-1}$–X $^5\Pi_{-1}$ system In total, 14 rotationally resolved bands of B $^5\Pi_{-1}$–X $^5\Pi_{-1}$ are observed, including (v'-0), (0-1), (1-2), and (3-3), where $v' = 0$–10. As an example, Fig. 3 shows the experimental and simulated spectra of B $^5\Pi_{-1}$–X $^5\Pi_{-1}$ (5-0). The spectrum is composed of P, Q, and R branches. The identifications of the P(2) and Q(1) lines conform to an $|\Omega'| = 1 - |\Omega''| = 1$ transition, where Ω is the projection of electronic angular momentum onto the internuclear axis. The long P-branch clearly splits into two components at high J'' due to the large Λ-doubling splitting (distinguished by e/f) in the upper state. Apart from this band, this splitting also occurs in other bands, seen in supplementary material. The Λ-doubling splitting of the ground electronic state is so tiny that the current experiment cannot identify the parities of e/f. Consequently, the e and f labels only represent the splitting observed from the Λ-doubling. Based on the fits of PEGOPHER, all the rotational constants of the upper and lower electronic states are listed in Table 1.

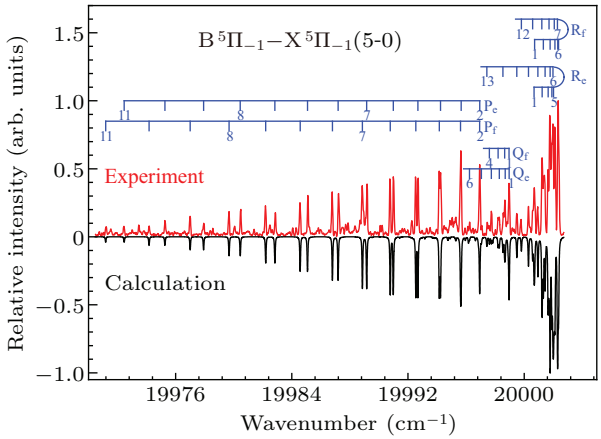


Fig. 3. Rotationally resolved B $^5\Pi_{-1}$–X $^5\Pi_{-1}$ (5-0) band of CrO. The top (red) trace represents the experimental observation, and the bottom (black) trace is the spectrum calculated from the molecular constants obtained from the rotational analysis. Totally, 54 transition lines are identified and fitted to an overall standard deviation of 0.0103 cm^{-1}.

Table 1. Molecular constants of the observed electronic states of CrO.

State	v	T_v	A	B_v	r_v	$D_v \times 10^5$	q_v	τ
X $^5\Pi$	0	0[a]	63.221[a]	0.524393(15)[a]		0.07258(25)[a]	0.0000333(29)[a]	
X $^5\Pi_{-1}$	0	0		0.5059(1)[b]	1.6507(2)[b]	–0.19(3)[b]	0.00009(4)[b]	
				0.5063[c]				
	1	885.811(4)		0.5016(2)	1.6578(4)	0.10(7)	0.0001(1)	
	2	1758.371(4)		0.4972(2)	1.6651(4)	0.42(8)	0.0001(1)	
	3	2617.560(4)		0.4928(3)	1.6725(6)	0.04(3)	0.0002(1)	
A $^5\Sigma^+$	0	8181.396(2)[a]		0.499203(15)[a]		0.06548(26)[a]		
A′ $^5\Delta$	0	11901.9042(18)[d]	53.2224(4)[d]	0.506525(10)[d]		0.0678(5)[d]		
	1	12780.1099(14)[d]	53.9517(4)[d]	0.502910(10)[d]		0.0702(10)[d]		
B $^5\Pi_{-1}$	0	16515.142(4)		0.4552(2)	1.7402(4)	–0.05(4)	–0.0024(1)	77(10)
	1	17249.020(4)		0.4499(2)	1.7504(4)	–0.75(4)	–0.0023(1)	75(10)
	2	17963.655(4)		0.4448(2)	1.7604(4)	–0.41(5)	–0.0027(1)	72(10)
	3	18662.040(4)		0.4392(1)	1.7716(3)	–0.18(4)	–0.0025(1)	92(10)
	4	19344.803(4)		0.4335(1)	1.7832(3)	–1.71(7)	–0.0014(1)	95(10)
	5	19999.103(4)		0.4344(1)	1.7814(3)	0.07(6)	–0.0069(1)	92(10)
	6	20652.290(4)		0.4235(1)	1.8042(3)	–0.08(7)	–0.0035(1)	95(10)
	7	21286.862(4)		0.4182(1)	1.8156(3)	–0.05(4)	–0.0022(1)	97(10)
	8	21907.594(4)		0.4130(1)	1.8270(3)	–0.49(8)	–0.0016(1)	98(10)
	9	22505.157(5)		0.4223(1)	1.8067(3)	1.67(9)	–0.0051(1)	97(10)
	10	23105.932(4)		0.4033(1)	1.8488(3)	–0.20(5)	–0.0025(1)	96(10)
B $^5\Pi_1$	1	17358.160(2)		0.4645(1)	1.7227(2)	–0.11(3)	–0.0035(1)	87(10)
	5	e: 20073.959(2)		e: 0.4644(1)	e: 1.7229(2)	e: 1.65(5)		
		f: 20073.995(5)		f: 0.5089(1)	f: 1.6458(2)	f: 2.21(5)		

Notes: Values in cm^{-1} except r_v and τ which are in Å and ns, respectively. Errors in parentheses are one standard deviation in units of the last significant figure quoted.
[a]Ref. [19]. [b]From a single global fit of the B $^5\Pi_{-1}$ ($v' = 0$–10)–X $^5\Pi_{-1}$ ($v'' = 0$) bands in this work. [c]Ref. [18]. [d]Ref. [20].

The equilibrium rotational and vibrational constants of both the $X\,^5\Pi_{-1}$ and $B\,^5\Pi_{-1}$ states are obtained by fitting the values of B_v and T_v to Eqs. (1) and (3), and the root-mean-square fitting errors are 0.00015 cm^{-1} and 0.93 cm^{-1} for the rotational and vibrational levels, respectively. The equilibrium bond length is calculated from B_e. Since the $B\,^5\Pi_{-1}$ ($v' = 5, 9$) states are perturbed (*vide infra*) in energy, their molecular parameters are not considered in the fits of B_v and T_v. Instead, the residuals between the observed vibrational energies and the values calculated from the fitted equilibrium molecular constants, i.e., (calc. − obs.), are labeled as ΔT, so as to identify the presence of the perturbation in the vibronic progression.

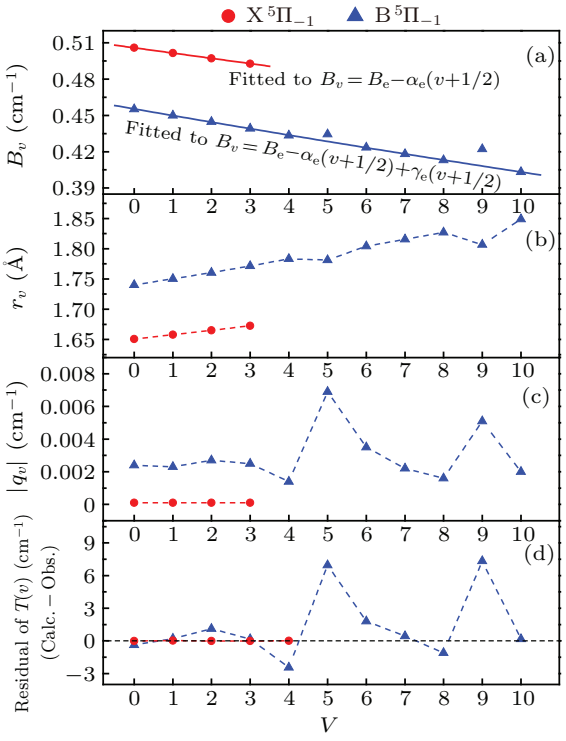


Fig. 4. Variations of the rotational constant (a) B_v, (b) bond length r_v, (c) Λ-doubling parameter q_v, and (d) vibrational energy residual (calc. − obs.) with vibrational quantum number v. The red circles and blue triangles indicate the ground $X\,^5\Pi_{-1}$ state and the excited $B\,^5\Pi_{-1}$ state, respectively. The solid lines are the results of the v-dependent fits, and the dashed lines are added to guide the reader's eyes.

Figure 4 visually shows how the rotational constants B_v, bond lengths r_v, Λ-doubling parameters q_v, and vibrational energy residuals ΔT vary as functions of the vibrational quantum number v in the $B\,^5\Pi_{-1}$ and $X\,^5\Pi_{-1}$ states. In Figs. 4(a) and 4(b), as expected in Morse potential, the rotational constants and bond lengths change smoothly as one goes to higher vibrational level, but irregular in the $B\,^5\Pi_{-1}$ ($v' = 5, 9$) states, indicating the possible existence of perturbations. In addition, an irregular Λ-doubling splitting is found in the $B\,^5\Pi_1$ ($v' = 5$) state (see next part) which is energetically close to the $B\,^5\Pi_{-1}$ ($v' = 5$) state, so there is possible interaction between these two states. However, there is no evidence in the current experiment to identify any state perturbing the $B\,^5\Pi_{-1}$ ($v' = 9$) state. In Figs. 4(c) and 4(d), the dramatic changes are found in the Λ-doubling splitting and vibrational energy of the $B\,^5\Pi_{-1}$ ($v' = 5, 9$) states, and the two variations have a very similar pattern, indicating that the perturbation effects on not only the rotational levels but also the Λ-doubling splitting and vibrational levels. According to the selection rules, the perturbations occurring may be attributed to the homogeneous interaction ($\Delta\Lambda = 0$) in Hund's case (a),[53,54] because the rotational structure in the $B\,^5\Pi_{-1}$ ($v' = 5, 9$) states regularly conforms to Eq. (2). In addition, the energy level shift induced by the perturbation is in the sense of the repulsion,[53] and the perturbed states $B\,^5\Pi_{-1}$ ($v' = 5, 9$) have the reduced vibrational energies and increased rotational constants. Therefore, the vibrational energy of the perturbing states should be higher than that of the corresponding observed state. Meanwhile, the bond length of the perturbing states may increase more than the expected value.

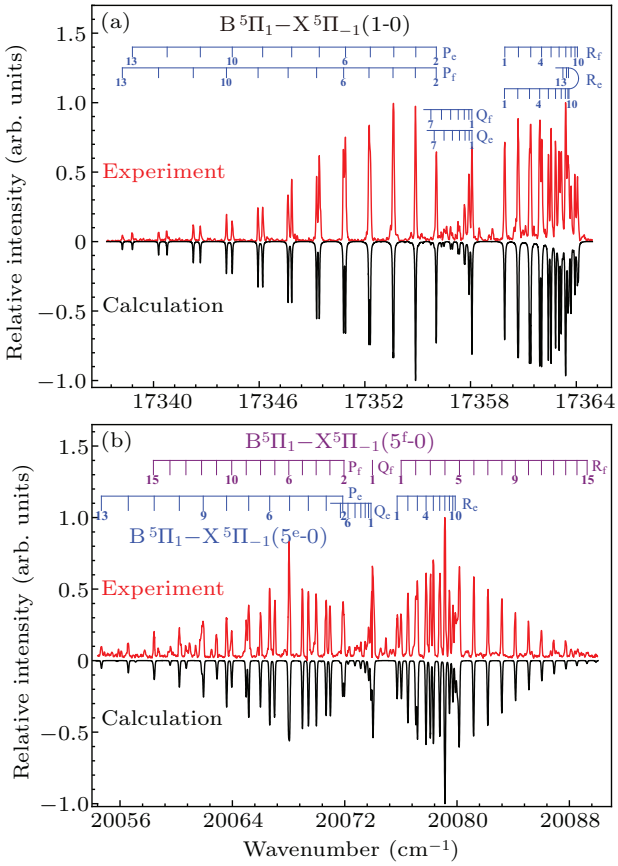


Fig. 5. Two rotationally resolved LIF excitation spectra of CrO. Panels (a) and (b) correspond to the (1-0) and (5-0) bands of the $B\,^5\Pi_1$–$X\,^5\Pi_{-1}$ transition, respectively. The top (red) trace represents the experimental observation, and the bottom (black) trace is the spectrum calculated from the molecular constants obtained from the rotational analysis. Totally, 115 transition lines are identified and fitted to an overall standard deviation of 0.0087 cm^{-1}.

B. The $B\,^5\Pi_1$–$X\,^5\Pi_{-1}$ system Two bands (1-0) and (5-0) are rotationally resolved in the $B\,^5\Pi_1$–$X\,^5\Pi_{-1}$ system, as shown in Fig. 5. The spectrum of the (1-0) band has obvious P, Q and R branches with the first lines P(2), Q(1), and R(1), indicating an $|\Omega'| = 1 - |\Omega''| = 1$ transition. The band

origin is 109.140 cm^{-1} above that of the B$^5\Pi_{-1}$–X$^5\Pi_{-1}$ (1-0) band, which reasonably accords with the estimated value of 106.865 cm^{-1} in Ref. [18]. The spectrum of the B$^5\Pi_1$–X$^5\Pi_{-1}$ (5-0) band is characteristic of two Λ-components of the upper state with irregular Λ-doubling splitting, so that we have to fit the spectra with individual Λ-component to Eq. (2). Finally, the two rotational constants, $B'(\mathrm{e}) = 0.4644$ cm^{-1} and $B'(\mathrm{f}) = 0.5089$ cm^{-1}, are obtained for the two Λ-components of the B$^5\Pi_1$ ($v' = 5$) state. Same as the discussion above, the labels e and f in the spectra only denote the two Λ-components, and cannot identify their parities.

As described above, the states B$^5\Pi_1$ ($v' = 5$) and B$^5\Pi_{-1}$ ($v' = 5$) are very close to each other in energy, and both of them have irregular changes of the molecular constants. Therefore, it is much possible that there is strong homogeneous interaction between these two states. However, because no transition to the B$^5\Pi_1$ ($v' = 2$–4 and $v' \geq 6$) states was observed in the experiment, it is also possible that the B$^5\Pi_1$ ($v' = 5$) state is perturbed by an unknown vibronic state which lends a favorable Franck–Condon factor to it.

3.2. SVL emission spectra of CrO

The SVL emission spectra of CrO are observed by dispersing the emitted fluorescence from a certain excited state. Three examples are shown in Figs. 6(a)–6(c), in which three vibrational progressions with energy levels $v'' = 0$–3 corresponding to the three spin–orbit components X$^5\Pi_{-1,0,1}$ are identified. The states X$^5\Pi_0$ ($v'' = 0$) and X$^5\Pi_1$ ($v'' = 0$) are measured by 56 cm^{-1} and 117 cm^{-1} above the ground X$^5\Pi_{-1}$ ($v'' = 0$) state, respectively. All of the observed vibrational levels from the SVL emission spectra are listed in Table 3, and the equilibrium vibrational constants ω_e and $\omega_e x_e$ are obtained by the fits of Eq. (1) and listed in Table 2. The fitting error of 0.36 cm^{-1} is smaller than the instrument accuracy (1 cm^{-1}), suggesting that no significant perturbation occurs in the observed vibrational levels X$^5\Pi_{-1}$ ($v'' = 0$–5), X$^5\Pi_0$ ($v'' = 0$–4), and X$^5\Pi_1$ ($v'' = 0$–3).

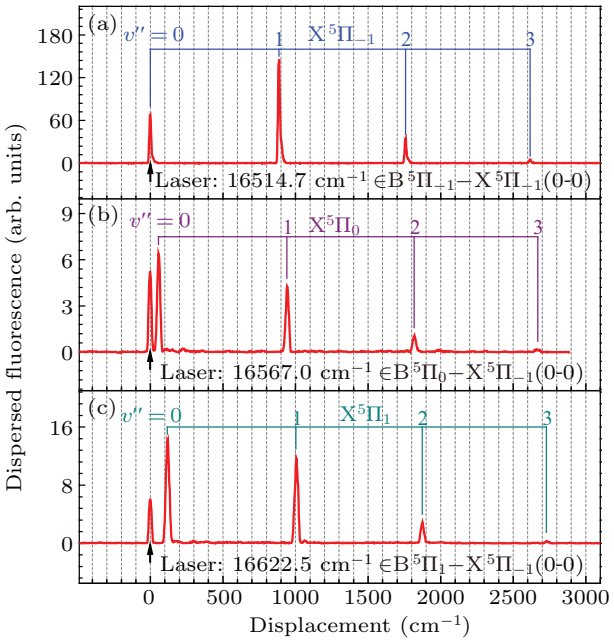


Fig. 6. SVL emission spectra of CrO. (a) Excitation laser is fixed at 16514.7 cm^{-1} of the B$^5\Pi_{-1}$–X$^5\Pi_{-1}$ (0-0) band; (b) excitation laser is fixed at 16567.0 cm^{-1} of the B$^5\Pi_0$–X$^5\Pi_{-1}$ (0-0) band; (c) excitation laser is fixed at 16622.5 cm^{-1} of the B$^5\Pi_1$–X$^5\Pi_{-1}$ (0-0) band. The x-axis shows the displacement in cm^{-1} from the position of the laser excitation.

Table 2. Equilibrium molecular constants of the B$^5\Pi_{-1}$ and X$^5\Pi_{-1}$ states for CrO.

State	B_e	α_e	$\gamma_e \times 10^5$	r_e	ω_e	$\omega_e x_e$	$\omega_e y_e$
X$^5\Pi_{-1}$	0.5081(1)	0.00437(2)		1.6471(1)	899.9(7)	6.9(1)	
	0.526643[a]	0.004434[a]		1.6179[a]	898.50[a]	6.72[a]	
X$^5\Pi_1$					899.7(8)	6.9(2)	
X$^5\Pi_0$					900.6(9)	7.5(3)	
B$^5\Pi_{-1}$	0.4582(3)	0.0056(1)	3.3(9)	1.7345(6)	754.2(1.6)	10.1(3)	0.14(2)
	0.473712[a]	0.005483[a]		1.7059[a]	752.81[a]	10.12[a]	

Notes: Values in cm^{-1} except r_e which is in Å. Errors in parenthese are one standard deviation in units of the last significant figure quoted. [a]Estimated values in Ref. [18].

Table 3. Vibrational energy levels (T_v, in cm^{-1}) of the ground electronic state of CrO from the SVL emission spectra.

	$v = 0$	$v = 1$	$v = 2$	$v = 3$	$v = 4$	$v = 5$
X$^5\Pi_{-1}$	0	886(1)	1758(1)	2617(1)	3463(1)	4293(1)
	0	885.811(5)[a]	1758.371(6)[a]	2617.560(7)[a]		
X$^5\Pi_0$	56(1)	941(1)	1814(1)	2672(1)	3516(1)	
	55.975[b]					
X$^5\Pi_1$	117(1)	1003(1)	1873(1)	2729(1)		
	117.074[b]					
X$^5\Pi_2$	182.819[b]	1066.538[c]	1937.683[c]			
X$^5\Pi_3$	252.757[b]	1135.295[c]	2005.892[c]			

Note: The numbers in the parentheses represent the uncertainties in the last digits.

[a]From the differences between the band origins of the rotationally resolved LIF excitation spectra.

[b]Measured in Ref. [19]. [c]Estimated in Ref. [18].

3.3. Radiative lifetimes of the excited states of CrO

The radiative decay resulting from laser exciting the rotationally resolved bands is obtained. As a typical example, Fig. 7 shows the observed (blue circles) and the fitted (red line) radiative decay curve from the $B\,^5\Pi_1$ ($v' = 1$) state. The observed decay trace represents an average about 8000 laser ablation pulses. The red decay curve is the fitting result with a first-order exponential function, showing a radiative lifetime $\tau = 87$ ns for the $B\,^5\Pi_1$ ($v' = 1$) state.

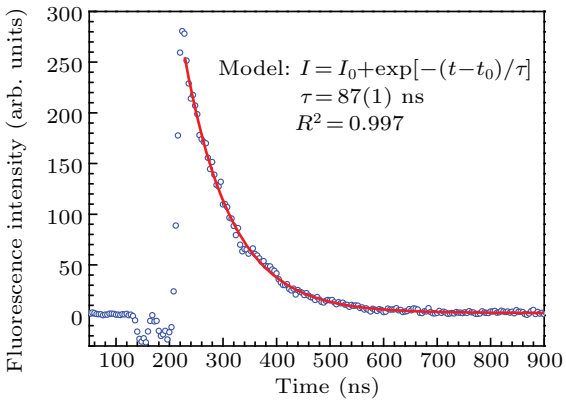


Fig. 7. Lifetime measurement of the $B\,^5\Pi_1$ ($v' = 1$) state. The open (blue) circles are experimental data, and the solid (red) line is an exponential fit of the fluorescence decay.

Table 1 lists the radiative lifetimes of all the observed vibronic states, ranging from 77 ns to 98 ns. These times are so short that the CrO molecules do not leave the observing window before they fluoresce completely, and thus the measured radiative lifetimes are adequately credible. Since the CrO molecule is carried by the supersonic jet, the measurement of the radiative lifetime is reasonably considered in a collisionless environment. Considering laser duration, fitting error, and system response time, the uncertainty of the measured lifetimes is expected to be 10 ns.

3.4. Overview of the electronic states of MoO and WO

Since the beginning of the last century, many experimental investigations on the electronic structures of other two Cr group metal monoxides, i.e., MoO[27–36] and WO,[37–50] were reported. Compared to CrO which strictly follows Hund's case (a) coupling scheme, the MoO and WO molecules tend to obey Hund's case (c) coupling scheme, where Ω, instead of Λ and S, is a good quantum number to describe the electronic states.

Tables 4 and 5 collects the major molecular constants of all the known electronic states of MoO and WO from the optical spectroscopic experiments. In Table 4, a total of 30 electronic states of MoO are provided, and the molecular constants were obtained from the resonant two-photon ionization spectra,[31] Fourier transform emission spectra,[34] and LIF excitation and SVL emission spectra.[35,36] Among these electronic states, the vibrational information is mainly limited in the low-energy electronic states, and the rotational information is mostly limited in the vibrational ground level. In Table 5, there are 25 electronic states containing 51 vibronic levels, which were obtained from the absorption spectra,[39] Fourier transform emission spectra,[48] LIF excitation spectra,[49,50] and SVL emission spectra.[51] Compared to MoO, many higher vibrational levels of WO possess rotational information. The average radiative lifetime of the excited states of WO is 247 ns. It is somewhat longer than that of CrO (89 ns) and much shorter than that of MoO (2.1 μs).

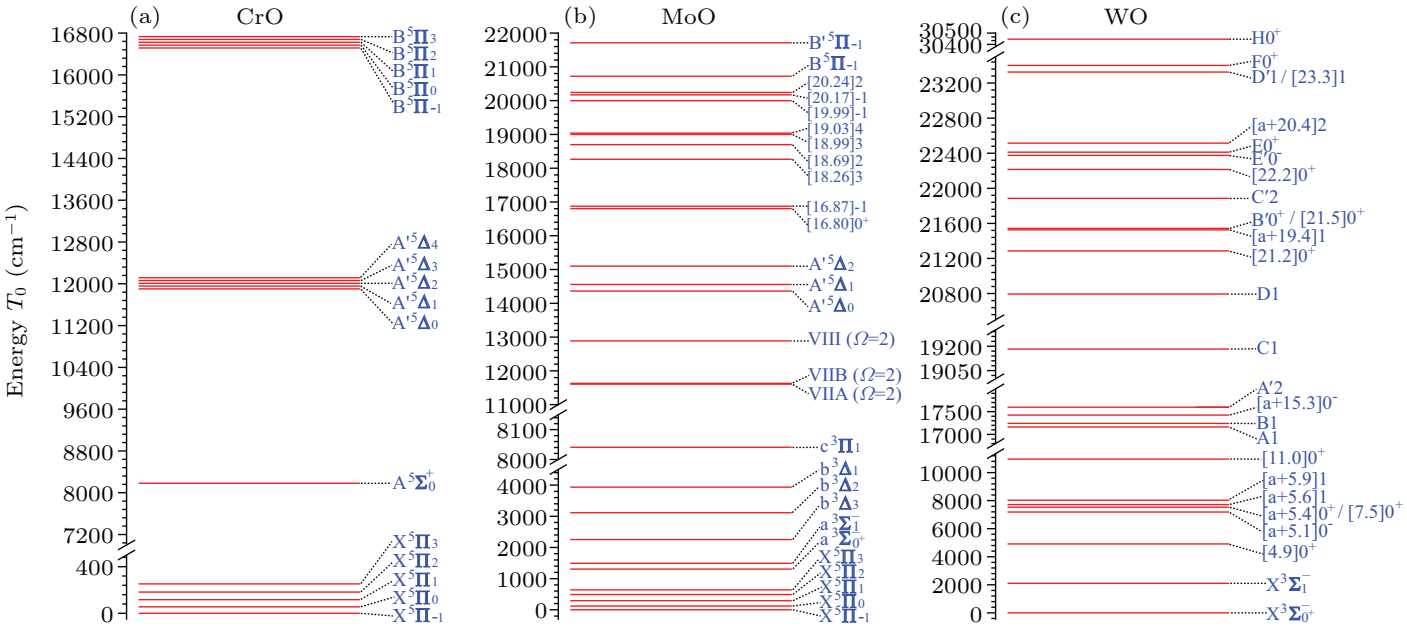


Fig. 8. Schematic energy level diagrams of CrO, MoO, and WO. The energies in cm^{-1} given are those for T_0, which are obtained from the optical spectra.

Table 4. Molecular constants of the experimentally known electronic states of MoO.

State	ω_e [$\Delta G_{1/2}$]	$\omega_e x_e$	v	T_v	B_v	r_v	$D_v \times 10^6$	q_v	τ
$X^5\Pi_{-1}$	917.1(1.4)[a]	1.8(4)[a]	0	0[a]	0.4180(1)[a]	1.7127(3)[a]		0.00062(14)[b]	
$X^5\Pi_0$	928.7(5)[c]	5.3(1)[c]	0	120(2)[c]	0.4233(3)[c]	1.704(1)[c]	3(1)[c]		
$X^5\Pi_1$	923(2)[c]	4.9(3)[c]	0	290(2)[c]					
$X^5\Pi_2$	1035.3(5)[c]	6.3(1)[c]	0	491(2)[c]	0.4249(5)[c]	1.701(2)[c]	7(3)[c]		
$X^5\Pi_3$			0	641(2)[c]	0.4306(2)[c]	1.690(1)[c]	1.2(3)[c]		
$a^3\Sigma^-_{0+}$	1013[c]	2.5[c]	0	1306(2)[c]	0.44645(14)[d]	1.6572(3)[e]	0.3[d]		
$a^3\Sigma^-_1$			0	1490(2)[c]					
$b^3\Delta_3$	913[c]	1.5[c]	0	2254(2)[c]					
$b^3\Delta_2$	[1016(3)][c]		0	3113(2)[c]					
$b^3\Delta_1$			0	3936(2)[c]					
$c^3\Pi_1$			0	8041(2)[d]	0.42495(14)[d]	1.6986(3)[e]	0.4201(25)[d]	–0.0006983(80)[d]	
VIIA ($\Omega = 2$)	799.40[f]	–13.70[f]	0	11605.7[b]	0.41164(44)[b]	1.726(1)[e]			650[b]
			1	12432.5[b]					840[b]
			2	13286.7[b]	0.40602(29)[b]	1.7378(7)[e]			580[b]
VIIB ($\Omega = 2$)	803.80[f]	–19.45[e]	0	11630.3[b]	0.42072(35)[b]	1.7071(8)[e]			1010[b]
			1	12473.0[b]	0.40625(46)[b]	1.737(1)[e]			900[b]
			2	13354.6[b]	0.40744(86)[b]	1.735(2)[e]			1100[b]
VIII ($\Omega = 2$)			0	12885.9[b]	0.41477(30)[b]	1.7193(7)[e]			1260[b]
$A'^5\Delta_0$	843.20[f]	–8.15[f]	0	14365.8[b]	0.39661(31)[b]	1.7583(7)[e]			4770[b]
			1	15225.3[b]	0.39122(19)[b]	1.7703(5)[e]			4420[b]
			2	16101.1[b]	0.39435(23)[b]	1.7633(6)[e]			4370[b]
$A'^5\Delta_1$			0	14557.0[b]	0.40515(9)[b]	1.7396(2)[e]			3910[b]
$A'^5\Delta_2$			0	15099.8[b]	0.42286(22)[b]	1.7028(5)[e]			4430[b]
[16.87]−1			0	16873.329(3)[c]	0.4117(2)[c]	1.7257(5)[e]	0.9(4)[c]	–0.0061(2)[c]	
[19.99]−1			0	19999.018(2)[c]	0.4158(1)[c]	1.7172(3)[e]	0.3(2)[c]		
[20.17]−1			0	20171.690(4)[c]	0.4029(3)[c]	1.7445(7)[e]	0.7(6)[c]	–0.0086(1)[c]	
[20.24]2			0	20242.540(5)[c]	0.4250(2)[c]	1.6986(4)[e]	2.1(4)[c]		
$[16.80]0^+$			0	16682.842(4)[c]	0.4045(3)[c]	1.7410(7)[e]	3(2)[c]		
[18.69]2			0	18205.584(8)[c]	0.4001(4)[c]	1.7506(9)[e]	7(3)[c]		
[18.26]3			0	17623.197(2)[c]	0.4214(1)[c]	1.7058(3)[e]	1.0(1)[c]		
[18.99]3			0	18357.826(2)[c]	0.4187(1)[c]	1.7113(3)[e]	0.8(2)[c]		
[19.03]4			0	18397.805(3)[c]	0.4273(1)[c]	1.6939(2)[e]	1.3(2)[c]		
[20.24]2			0	19601.541(4)[c]	0.4248(2)[c]	1.6989(4)[e]	2.1(3)[c]		
$B^5\Pi_{-1}$	777.10[f]	6.75[f]	0	20723.2[b]	0.39293(17)[b]	1.7665(4)[e]		0.01872(16)[b]	370[b]
$B^5\Pi_0$			1	21642(2)[g]	0.37686(24)[b]	1.8038(6)[e]			
$B'^5\Pi_{-1}$			0	21712.1[b]	0.40644(18)[b]	1.7369(4)[e]		–0.01998(16)[b]	270[b]

Notes: Values in cm^{-1} except bond length r_e and lifetime τ which are in Å and ns, respectively. The molecular constants of the $^{98}Mo^{16}O$ isotopologue are provided when the spectra were isotopically resolved in Refs. [31,36]. The numbers in the parentheses represent the uncertainties in the last digits, and the value in square bracket is the $\Delta G_{1/2}$ value.

[a]Ref. [36], [b]Ref. [31], [c]Ref. [35], [d]Ref. [34], [e]obtained by $r_v = [h/(8\pi^2\mu B_v)]^{1/2}$.

[f]Fitted by Eq. (1). [g]Obtained by $T_v = \nu_0 + 120$, where ν_0 is the band origin from Ref. [31] and the value of 120 is T_0 of $X^5\Pi_0$.

Table 5. Molecular constants of the experimentally known electronic states of WO.

State	ω_e [$\Delta G_{1/2}$]	$\omega_e x_e$	v	T_v	B_v	r_v	$D_v \times 10^6$	q_v	τ
$X^3\Sigma^-_{0+}$	1065.5951(71)[a]	4.0103(40)[a]	0	0[a]	0.4155370(54)[a]	1.66038(2)[b]	0.2554(15)[a]		
			1	1057.56542(86)[a]	0.4135229(53)[a]	1.66442(2)[c]	0.2570(14)[a]		
			2	2107.0887(15)[a]	0.4114968(56)[a]	1.66851(2)[c]	0.2589(16)[a]		
			3	3148.5456(24)[a]	0.4094774(65)[a]	1.67262(2)[c]	0.2639(20)[a]		
			4	4181.9326(31)[a]	0.4074382(72)[a]	1.67680(2)[c]	0.2636(22)[a]		
$X^3\Sigma^-_1$	1067.9939(34)[a]	4.0314(16)[a]	0	2103.15(2)[b]	0.4162385(89)[a]	1.65898(2)[b]	0.2480(24)[a]	0.00016254(56)[a]	
			1	3163.08(2)[d]	0.4142196(90)[a]	1.66302(2)[c]	0.2484(25)[a]	0.00016228(36)[a]	
			2	4214.95(2)[d]	0.412195(10)[a]	1.66710(3)[c]	0.2487(31)[a]	0.000162[a]	
$[4.9]0^+$			0	4910.6260(49)[a]	0.403506(18)[a]	1.68495(4)[b]	0.409(45)[a]		
$[a+5.1]0^-$			0	7189.20(2)[b]	0.3926388(73)[a]	1.70811(2)[b]	0.1645(48)[a]		
$[a+5.4]0^+$ or $[7.5]0^+$	[954.3081(50)][a]		0	7537.8417(18)[a]	0.3919096(79)[a]	1.70970(2)[b]	0.2434(56)[a]		
			1	8492.1470(48)[a]	0.389984(10)[a]	1.71392(3)[c]	0.2625(35)[a]		
[a+5.6]1			0	7720.42(2)[b]	0.3946026(46)[a]	1.70386(1)[b]	0.1996(38)[a]	0.0012810(35)[a]	
[a+5.9]1			0	8029.95(2)[b]	0.3948424(65)[a]	1.70334(2)[b]	0.1998(52)[a]	–0.0025222(22)[a]	
$[11.0]0^+$	[1023.7031(32)][a]		0	10965.4450(19)[a]	0.4151496(68)[a]	1.66116(2)[b]	0.2726(22)[a]		
			1	11989.1481(26)[a]	0.411745(20)[a]	1.66801(5)[c]	0.308(37)[a]		
A1	927.2141(23)[a]	10.2157(16)[a]	0	17164.9641(14)[a]	0.3913397(73)[a]	1.71094(2)[b]	2.1370(60)[a]	0.0034260(57)[a]	
			1	18074.2157(16)[a]	0.3847932(81)[a]	1.72544(2)[c]	0.8175(58)[a]	0.0046229(78)[a]	
			2	18969.8725(19)[a]	0.3816100(76)[a]	1.73262(2)[c]	0.5054(37)[a]	0.0047594(58)[a]	
			3	19856.4924(16)[a]	0.3790911(64)[a]	1.73836(2)[c]	0.3848(27)[a]	0.0047344(49)[a]	

Table 5. (Continued).

State	ω_e [$\Delta G_{1/2}$]	$\omega_e x_e$	v	T_v	B_v	r_v	$D_v \times 10^6$	q_v	τ
B1	988.4476(47)[a]	1.2865(20)[a]	0	17242.0010(14)[a]	0.3923935(84)[a]	1.70865(2)[b]	–1.6677(88)[a]	0.0041865(81)[a]	
			1	18227.8756(22)[a]	0.3897094(99)[a]	1.71452(3)[c]	–0.7249(76)[a]	–0.0052[a]	
			2	19211.7718(19)[a]	0.386997(14)[a]	1.72052(4)[c]	–2.162(32)[a]	0.014162(21)[a]	
[a+15.3]0$^-$			0	17424.84(2)[b]	0.3911750(57)[a]	1.71130(2)[b]	0.4939(44)[a]		
A′2	[911.5639(46)][a]		0	17597.11(2)[b]	0.386440(30)[a]	1.72176(7)[b]	0.242(33)[a]		
			1	18508.67(2)[a]	0.384924(10)[a]	1.72514(3)[c]	0.2831(58)[a]		
C1	932.5699(54)[a]	2.6613(21)[a]	0	19182.4617(15)[a]	0.3914117(71)[a]	1.71079(2)[c]	0.2498(53)[a]	–0.0000190(29)[a]	
			1	20109.7092(22)[a]	0.388227(12)[a]	1.71779(3)[c]	0.802(22)[a]	0.001461(13)[a]	
			2	21031.6341(31)[a]	0.3879669(90)[a]	1.71836(2)[c]	0.6373(70)[a]	–0.0024792(62)[a]	
D1	990.1374(33)[a]	5.5198(13)[a]	0	20793.8569(11)[a]	0.3889130(59)[a]	1.71627(2)[b]	0.2436(20)[a]	–0.0002469(27)[a]	356(10)[e]
			1	21772.9832(15)[a]	0.3870643(58)[a]	1.72037(2)[c]	0.2611(18)[a]	–0.0002808(28)[a]	
			2	22741.5033(12)[a]	0.3852613(59)[a]	1.72439(2)[c]	0.3003(19)[a]	–0.0006125(49)[a]	
			3	23699.8391(14)[a]	0.3831108(55)[a]	1.72922(2)[c]	0.3004(15)[a]	–0.0005615(22)[a]	
[21.2]0$^+$	819.1(6)[e]	16.3(4)[e]	0	21286.73(2)[f]	0.3845(1)[f]	1.7260(3)[f]	4.8(3)[f]		473(10)[e]
			1	22089.29(2)[f]	0.3837(1)[f]	1.7278(4)[f]	3.3(6)[f]		
[a+19.4]1			0	21525.32(2)[a]	0.3750801(73)[a]	1.74764(2)[b]	0.1459(45)[a]	–0.0001670(30)[a]	
B′0$^+$ or [21.5]0$^+$	950.6(6)[e]	4.7(3)[e]	0	21542.786(2)[e]	0.3854840(89)[a]	1.72389(2)[b]	0.2657(24)[a]		198(10)[e]
			1	22489.52(2)[e]	0.3835848(99)[a]	1.72815(3)[c]	0.2624(29)[a]		153(10)[e]
			2	23426.08(3)[e]	0.3822(7)[e]	1.7315(8)[e]			149(10)[e]
C′2	[939.5164(26)][a]		0	21885.94(2)[b]	0.3879773(89)[a]	1.71834(2)[b]	0.2703(24)[a]		230(10)[e]
			1	22825.35(2)[d]	0.386097(10)[a]	1.72252(3)[c]	0.2759(32)[a]		
[22.2]0$^+$			0	22214.73(1)[f]	0.3803(1)[f]	1.7352(3)[f]	0.63(7)[f]		303(10)[e]
			1	23173.67(3)[f]	0.3782(3)[f]	1.7401(7)[f]	3.5(9)[f]		365(10)[e]
E′0$^-$			0	22375.36(2)[b]	0.384305(18)[a]	1.72653(5)[b]	0.343(21)[a]		
E0$^+$			0	22412.194(11)[a]	0.385625(26)[a]	1.72357(6)[b]	0.166(13)[a]		231(10)[e]
[a+20.4]2			0	22514.53(2)[b]	0.377243(56)[a]	1.7426(2)[b]	0.1550(38)[a]		
D′1 or [23.3]1			0	23325.45(2)[b]	0.3849270(88)[a]	1.72514(2)[b]	0.2866(24)[a]	–0.0011572(27)[a]	175(10)[e]
F0$^+$	[917.4443(33)][a]		0	23401.0801(28)[a]	0.383930(12)[a]	1.72738(3)[b]	0.467(11)[a]		84(10)[e]
			1	24318.5243(17)[a]	0.3811162(62)[a]	1.73374(2)[c]	0.2855(19)[a]		
H0$^+$	[903.915(363)][g]		0	30445.852(347)[g]	0.388712(225)[g]	1.7167(5)[b]	0.732(27)[g]		
			1	31349.767(107)[g]	0.384709(68)[g]	1.7256(2)[c]	0.222(8)[g]		

Notes: Values in cm^{-1} except bond length r_e and lifetime τ which are in Å and ns, respectively. The molecular constants of the $^{184}W^{16}O$ isotopologue are provided when the spectra were isotopically resolved in Refs. [48,50]. The numbers in the parentheses represent the uncertainties in the last digits, and the values in square brackets are the $\Delta G_{1/2}$ values.

[a]Ref. [48], [b]Ref. [51], [c]obtained by $r_v = [h/(8\pi^2 \mu B_v)]^{1/2}$.

[d]Obtained by $T_v = v_0 + 2103.15$, where v_0 is the band origin from Ref. [48] and the value of 2103.15 is the spin–orbit splitting of the ground electronic state from Ref. [51]. [e]Ref. [49], [f]Ref. [50], [g]from $^{186}W^{16}O$ in Ref. [39].

Based on Tables 1, 4, and 5, Fig. 8 constructs the electronic energy level diagram of the Cr group metal monoxides. The electronic states are energetically represented by the ground vibrational level. Compared to CrO, the MoO and WO molecules have more plentiful and complex electronic states, because Hund's case (c) coupling scheme causes the extensive appearances of the Ω-components of the electronic states. Therefore, many observed states of MoO and WO were only identified by the Ω values, instead of the explicit assignments.

4. Discussion

4.1. Electronic configurations of the Cr group metal monoxides

For the Cr group transition metal monoxides, the characteristics of the low-lying electronic states can be qualitatively analyzed with the simplified molecular orbital diagram, which involves the valence 2s and 2p orbitals of the O atom and the valence nd and $(n+1)$s orbitals of the metal atom, as shown in Fig. 9.

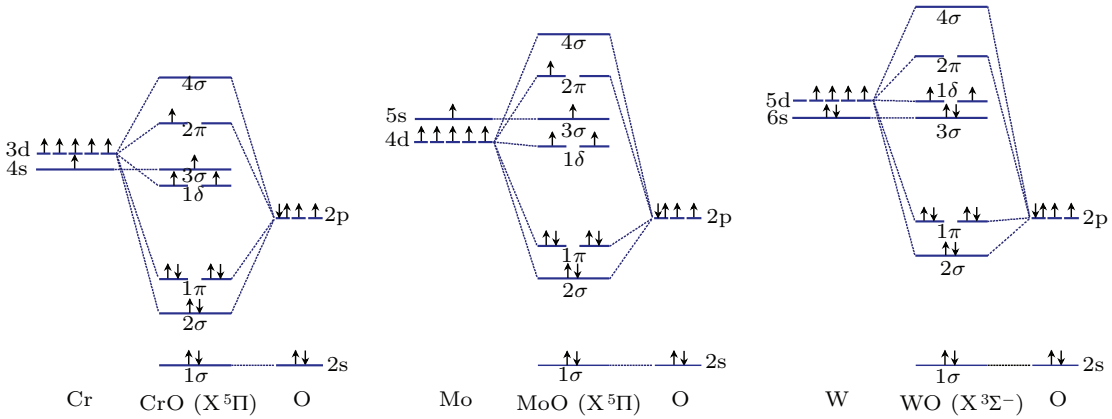


Fig. 9. Molecular orbital diagrams of the Cr group transition metal monoxides: (a) CrO, (b) MoO, (c) WO.

The molecular orbitals are drawn on a rough energy scale, and are organized by the bonding 2σ and 1π orbitals, the nonbonding 1σ, 3σ and 1δ orbitals, and the antibonding 2π and 4σ orbitals. With increasing energy, the molecular orbitals of CrO and MoO are composed of the following order 1σ, 2σ, 1π, 1δ, 3σ, 2π, 4σ, while the 3σ and 1δ orbitals in WO lie quite close and the order is reversed due to the strong relativistic effect in the W atom. For the valence molecular orbitals, the three lowest orbitals are fully filled, and hence the electronic occupation of the rest of orbitals dominants the electronic structures of the ground and low-lying electronic states.

For the CrO molecule, the electronic configuration of the ground electronic state is $1\delta^2 3\sigma^1 2\pi^1$, $X^5\Pi$. Above the ground electronic state, Table 1 presents three excited electronic states having the same spin multiplicity, i.e., $A^5\Sigma^+$, $A'^5\Delta$, and $B^5\Pi$. Here, the $A^5\Sigma^+$ state has the electronic configuration of $1\delta^2 2\pi^2$, formed from the promotion of the 3σ electron to the 2π orbitals. The configuration of $A'^5\Delta$ is $1\delta^1 3\sigma^1 2\pi^2$, corresponding to the promotion of an electron from the 1δ to 2π orbitals. In the spectroscopic experiments, the $A'^5\Delta$ state is observed 3721 cm^{-1} higher than the $A^5\Sigma^+$ state, so that the 3σ molecular orbital lies above the 1δ orbitals. The $B^5\Pi$ state, investigated in this work, has the $1\delta^2 2\pi^1 4\sigma^1$ configuration, corresponding to the promotion of an electron in the ground electronic state from the nonbonding 3σ orbital to the antibonding 4σ orbital. Therefore, it is reasonable that the bond length increases and the vibrational frequency decreases when comparing the molecular parameters of the $B^5\Pi$ state to those of the ground $X^5\Pi$ state. In addition, the promotion from 3σ to 4σ carries the largest oscillator, so the B–X transition is the strongest one compared to the transitions A–X and A′–X.

The significance of the relativistic effect can be illustrated by the electronic structures of the MoO and WO molecules. The electronic configuration of the ground electronic state of MoO is the same as that of CrO, i.e., $1\delta^2 3\sigma^1 2\pi^1$ ($X^5\Pi$), while WO has an $X^3\Sigma^-$ ground electronic state and the configuration of $3\sigma^2 1\delta^2$. The difference is due to the significant relativistic effect in the W atom which causes the 6s atomic orbital to contract dramatically and the 5d orbitals to expend slightly. In other words, because of the mass-velocity effect (relativistic effect) in a classical picture of a heavy atom, for example W atom, the velocities of the penetrating 6s electrons near to the nucleus become very large, causing the 6s orbital to contract and drop in energy. Meanwhile, the nonpenetrating 5d electrons are shielded from the nuclear charge more effectively after the contraction of the 6s orbital, causing the 5d orbitals to expand and move higher in energy. For the WO molecule, it is reasonable that the 3σ orbital lies lower than the 1δ orbitals, resulting in the different electronic configuration from CrO and MoO.

4.2. Relativistic effect in the 5d transition metal monoxides

The electronic states of other 5d transition metal monoxides are also influenced by the relativistic effect and have the similar changes to the ground electronic configurations from MoO to WO. Table 6 collects the ground electronic term and the electronic configuration of all the transition metal monoxides, as well as the spin–orbit splitting, bond length, and vibrational frequency. As a conclusion, the ground electronic terms and configurations of the 4d transition metal monoxides are the same as those of the corresponding 3d transition metal monoxides, except the differences emerging in the groups 4 and 9. For the metal atoms of groups 5–9, the ground electronic terms and configurations of the 5d metal monoxides are different to those of the corresponding 4d or 3d metal monoxides.

Another manifestation of the relativistic effect in the 5d transition metal monoxides is the shortened bond length of the ground electronic state. This is visually drawn in Fig. 10, where the bond length (r_0) values are taken from Table 6. The bond lengths of the 4d transition metal monoxides are obviously longer than those of the corresponding 3d metal monoxides, and the trends of the two period species follow similar pattern. However, due to the strong relativistic effect in the 5d transition metals, the bond lengths of the 5d transition metal monoxides are significantly shrunken, comparing to the bond length increasing from the 3d to 4d period species. As seen in the figure, the transition metals from Nb/Ta to Rh/Ir and the metals heavier than Rh/Ir, the bond lengths of the 5d transition metal monoxides are even shorter than those of the corresponding 4d transition metal monoxides, and a ring-like structure is constituted here. Interestingly, the changes in the ground electronic configurations from the 4d to 5d transition metal monoxides also occur in the species inside the ring-like region.

In addition, according to the equation of vibrational frequency $\omega_e = (k/\mu)^{1/2}$,[53] where μ is the reduced mass and k is the force constant, the vibrational frequencies of the same group metal monoxides should decrease as the metal increases from 3d to 5d. The previous work has pointed out that the strong relativistic effect could increase the force constant, and even resulted in the increase of vibrational frequency from 4d to 5d transition metal monoxides.[108] Thus, the relativistic effect in the 5d transition metal monoxides can also be significantly reflected in the trends of the vibrational frequencies of the same group metal monoxides, such as AuO (646 cm^{-1}) > CuO (633 cm^{-1}) > AgO (491 cm^{-1}). For the metal atoms heavier than those of group 5, the vibrational frequencies of the monoxides have very similar pattern, especially the vibrational frequencies of the 5d transition metal monoxides are all higher than those of the corresponding 4d transition metal monoxides.

Table 6. The ground electronic term and configuration and the measured molecular constants of the ground electronic state for all of the transition metal monoxides.

Information of the ground state	3 IIIB	4 IVB	5 VB	6 VIB	7 VIIB	8	9 VIIIB	10	11 IB	12 IIB
3d-monoxids[a]	ScO	TiO	VO	CrO	MnO	FeO	CoO	NiO	CuO	ZnO
Ground electronic term	$X^2\Sigma^+$	$X^3\Delta_1$	$X^4\Sigma^-$	$X^5\Pi_{-1}$	$X^6\Sigma^+$	$X^5\Delta_4$	$X^4\Delta_{7/2}$	$X^3\Sigma^-_{0+}$	$X^2\Pi_{3/2}$	$X^1\Sigma^+$
Configuration	σ^1	$\sigma^1\delta^1$	$\sigma^1\delta^2$	$\sigma^1\delta^2\pi^1$	$\sigma^1\delta^2\pi^2$	$\sigma^1\delta^3\pi^2$	$\sigma^2\delta^3\pi^2$	$\sigma^2\delta^4\pi^2$	$\sigma^2\delta^4\pi^3$	$\sigma^2\delta^4\pi^4$
Spin–orbit splitting, A (cm^{-1})		96		63		190	332	50	277	
Bond length, r_0 (Å)	1.668	1.623	1.592	1.650	1.648	1.629	1.636	1.631	1.724	1.708
Vibrational frequency, ω_e (cm^{-1})	972	1009	1011	899	840	881	851	839	633	720
4d-monoxids[b]	YO	ZrO	NbO	MoO	TcO	RuO	RhO	PdO	AgO	CdO
Ground electronic term	$X^2\Sigma^+$	$X^1\Sigma^+$	$X^4\Sigma^-$	$X^5\Pi_{-1}$	($X^6\Sigma^+$)	$X^5\Delta_4$	$X^4\Sigma^-$	$X^3\Sigma^-_{0+}$	$X^2\Pi_{3/2}$	($X^1\Sigma^+$)
Configuration	σ^1	σ^2	$\sigma^1\delta^2$	$\sigma^1\delta^2\pi^1$	($\sigma^1\delta^2\pi^2$)	$\sigma^1\delta^3\pi^2$	$\sigma^1\delta^4\pi^2$	$\sigma^2\delta^4\pi^2$	$\sigma^2\delta^4\pi^3$	($\sigma^2\delta^4\pi^4$)
Spin–orbit splitting, A (cm^{-1})			62	160		399			269	
Bond length, r_0 (Å)	1.790	1.714	1.685	1.712	(1.737)	1.717	1.717	(1.815)	2.005	(1.920)
Vibrational frequency, ω_e (cm^{-1})	862	977	990	918	(900)	869	805	(671)	491	645
5d-monoxids[c]	LaO	HfO	TaO	WO	ReO	OsO	IrO	PtO	AuO	HgO
Ground electronic term	$X^2\Sigma^+$	$X^1\Sigma^+$	$X^2\Delta_{3/2}$	$X^3\Sigma^-_{0+}$	$X^2\Delta_{5/2}$	($X^5\Sigma^+$)	$X^2\Delta_{5/2}$	$X^3\Sigma^-_{0+}$	$X^2\Pi_{3/2}$	($X^1\Sigma^+$)
Configuration	σ^1	σ^2	$\sigma^2\delta^1$	$\sigma^2\delta^2$	$\sigma^2\delta^3$	($\sigma^2\delta^2\pi^2$)	$\sigma^2\delta^3\pi^2$	$\sigma^2\delta^4\pi^2$	$\sigma^2\delta^4\pi^3$	($\sigma^2\delta^4\pi^4$)
Spin–orbit splitting, A (cm^{-1})			3506	2103				936	1467	
Bond length, r_0 (Å)	1.828	1.726	1.689	1.660	1.644	1.688	1.726	1.730	1.853	(1.910)
Vibrational frequency, ω_e (cm^{-1})	817	974	1029	1066	1009	885	909	851	646	(613)

Note: When no experimental data exist, computational results are provided in the parentheses.

[a]3d-monoxides: ScO from Refs. [57,58]; TiO from Refs. [59–61]; VO from Refs. [62,63]; CrO from Refs. [18,19]; MnO from Ref. [64]; FeO from Refs. [12,65]; CoO from Refs. [12,66]; NiO from Refs. [67,68]; CuO from Refs. [69,70]; ZnO from Refs. [71,72].

[b]4d-monoxides: YO from Refs. [73–75]; ZrO from Refs. [59,76]; NbO from Refs. [77–79]; MoO from Refs. [31,35]; TcO from Ref. [80]; RuO from Refs. [81,82]; RhO from Refs. [83,84]; PdO from Refs. [85,86]; AgO from Refs. [87,88]; CdO from Refs. [89,90].

[c]5d-monoxides: LaO from Refs. [91,92]; HfO from Refs. [59,93]; TaO from Refs. [94,95]; WO from Refs. [48,51]; ReO from Refs. [96,97]; OsO from Refs. [98,99]; IrO from Ref. [100]; PtO from Refs. [101–103]; AuO from Refs. [104–106]; HgO from Refs. [90,107].

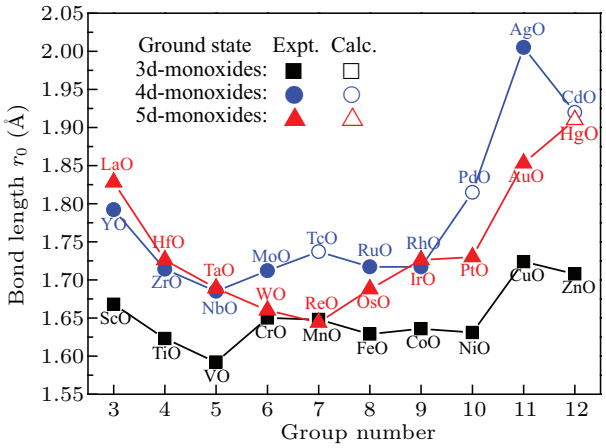


Fig. 10. Trends of the experimental (solid points) and computational (hollow points) bond lengths of the ground states for the 3d transition metal monoxides (black), 4d transition metal monoxides (blue), and 5d transition metal monoxides (red). The solid lines are added to guide the reader's eyes.

5. Conclusion

The LIF excitation and SVL emission spectra of the jet-cooled CrO molecule were observed. In the LIF excitation spectra, 16 vibronic bands were rotationally resolved in the energy range of 13800–23200 cm^{-1}. By the rotational analysis of the excitation spectra, the rotational constants of the upper $B\,^5\Pi_{-1}$ ($v' = 0$–10) and $B\,^5\Pi_1$ ($v' = 1, 5$) states and lower $X\,^5\Pi_{-1}$ ($v'' = 0$–3) states were obtained. By the vibrational analysis of the emission spectra, the vibrational constants of the three spin–orbit components $X\,^5\Pi_{-1,0,1}$ in the ground electronic state were obtained. Additionally, the radiative lifetimes of the vibronic states $B\,^5\Pi_{-1}$ ($v' = 0$–10) were measured by fitting the time-resolved fluorescence decay.

With the inclusion of CrO, a comprehensive database for the spectroscopic information of the Cr group metal monoxides (CrO, MoO and WO) has been provided to show the electronic structures in the ground and low-lying electronic states. In addition, the spectroscopic information on the ground electronic state of all the transition metal monoxides has been collected, including the electronic configuration, spin–orbit splitting, bond length, and vibrational frequency. It is argued that the shortening in the bond lengths and increasing in the vibrational frequencies of the 5d transition metal monoxides result from the relativistic contraction of the 6s orbital and expansion of the 5d orbital in the 5d transition metal atoms.

Data availability statement

The data that support the findings of this study are openly available in Science Data Bank at https://doi.org/10.57760/sciencedb.j00113.00085.

Acknowledgements

Project supported by the National Key R&D Program of China (Grant No. 2022YFA1602500), the National Natural Science Foundation of China (Grant No. 12027809), and Strategic Priority Research Program of the Chinese Academy of Sciences (Grant No. XDB21030900).

References

[1] Aoto Y A, de Lima Batista A P, Köhn A and de Oliveira-Filho A G S 2017 *J. Chem. Theory. Comput.* **13** 5291
[2] Claveau E E and Miliordo E 2019 *Phys. Chem. Chem. Phys.* **21** 26324
[3] Smirnov A N, Solomonik V G, Yurchenko S N and Tennyson J 2019 *Phys. Chem. Chem. Phys.* **21** 22794
[4] Morse M D 2019 *Acc. Chem. Res.* **52** 119
[5] Sorensen J J, Ewigleben J C, Tieu E, Sevy A, Merriles D M, Nielson C and Morse M D 2020 *J. Chem. Phys.* **153** 074303
[6] Merriles D M, Sevy A, Nielson C and Morse M D 2020 *J. Chem. Phys.* **153** 024303
[7] Bai X L, Zhang X D, Zhang F Q and Steimle T C 2022 *Chin. Phys. B* **31** 053301
[8] Davis D N 1947 *Astrophys. J.* **106** 28
[9] Kamiński T, Mason E, Tylenda R and Schmidt M R 2015 *Astron. Astrophys.* **580** A34
[10] Humphreys R M, Ziurys L M, Bernal J J, Gordon M S, Helton L A, Ishibashi K, Jones T J, Richards A M S and Vlemmings W 2019 *Astrophys. J. Lett.* **874** L26
[11] Pastorello A, Mason E and Taubenberger S 2019 *Astron. Astrophys.* **630** A75
[12] Merer A J 1989 *Annu. Rev. Phys. Chern.* **40** 407
[13] Gong Y, Zhou M and Andrews L 2009 *Chem. Rev.* **109** 6765
[14] Eder J M and Valenta E 1911 *Atlas Typischer Spektren* (Wienna, Alfred Hölder)
[15] Ferguson W F C 1932 *J. Res. Natl. Bur. Stand.* **8** 381
[16] Ninomiya M 1955 *J. Phys. Soc. Jpn.* **10** 829
[17] Weltner, Jr. W 1967 *Science* **155** 155
[18] Hocking W H, Merer A J, Milton D J, Jones W E and Krishnamurt G 1980 *Can. J. Phys.* **58** 516
[19] Cheung A S C, Żyrnicki W and Merer A J 1984 *J. Mol. Spectrosc.* **104** 315
[20] Barnes M, Hajigorgiou P G and Merer A J 1993 *J. Mol. Spectrosc.* **160** 289
[21] Wenthold P G, Gunion R F and Lineberger W C 1996 *Chem. Phys. Lett.* **258** 101
[22] Hedgecock I M, Naulin C and Costes M 1996 *Chem. Phys.* **207** 379
[23] Hedgecock I M, Naulin C and Costes M 1997 *J. Mol. Spectrosc.* **184** 462
[24] Gutsev G L, Jena P, Zhai H J and Wang L S 2001 *J. Chem. Phys.* **115** 7935
[25] Sheridan P M, Brewster M A and Ziurys L M 2002 *Astrophys. J.* **576** 1108
[26] Bauschlicher Jr C W, Nelin C J and Bagus P S 1985 *J. Chern. Phys.* **82** 3265
[27] Nelin C J and Bauschlicher Jr C W 1985 *Chem. Phys. Lett.* **118** 221
[28] Cooper G A, Gentleman A S, Iskra A and Mackenzie S R 2017 *J. Chem. Phys.* **147** 013921
[29] Picardi G 1933 *Atti Accad. Lincei* **17** 654
[30] Bates J K and Gruen D M 1979 *J. Mol. Spectrosc.* **78** 284
[31] Hamrick Y M, Taylor S and Morse M D 1991 *J. Mol. Spectrosc.* **146** 274
[32] Gunion R F, Dixon-Warren S J, Lineberger W C and Morse M D 1996 *J. Chem. Phys.* **104** 1765
[33] Kuzyakov Y Y, Moskvitina E N and Filippova E N 1997 *Spectrosc. Lett.* **30** 1057
[34] Harms J C, Womack K A, O'Brien L C and Zou W 2014 *J. Chem. Phys.* **141** 134310
[35] Zhang L, Zou W, Yu Y, Zhao D, Ma X and Yang J 2021 *J. Quant. Spectrosc. Radiat. Transf.* **269** 107690
[36] Zhang L, Yu Y, Qian D, Zhao D, Ma X and Yang J 2022 *J. Quant. Spectrosc. Radiat. Transf.* **277** 107962
[37] Gatterer A and Krishnamurty S G 1952 *Nature* **169** 543
[38] Weltner W and McLeod D 1965 *J. Mol. Spectrosc.* **17** 276
[39] Samoilova A N, Efremov Y M and Gurvich L V 1981 *J. Mol. Spectrosc.* **86** 1
[40] Green D W and Ervin K M 1981 *J. Mol. Spectrosc.* **89** 145
[41] Nelin C J and Bauschlicher C W 1985 *Chem. Phys. Lett.* **118** 221
[42] Kuzyakov Y Y, Moskvitina E N and Filippova E M 1997 *Spectrosc. Lett.* **30** 1057
[43] Kuzyakov Y Y, Moskvitina E N and Filippova E M 1998 *Chem. Phys. Reports* **17** 841
[44] Kraus D, Saykally R J and Bondybey V E 1998 *Chem. Phys. Lett.* **295** 285
[45] Lorenz M, Agreiter J, Caspary N and Bondybey V E 1998 *Chem. Phys. Lett.* **291** 291
[46] Lorenz M and Bondybey V E 1999 *Chem. Phys.* **241** 127
[47] Ram R S, Liévin J, Li G, Hirao T and Bernath P F 2001 *Chem. Phys. Lett.* **343** 437
[48] Ram R S, Liévin J and Bernath P F 2009 *J. Mol. Spectrosc.* **256** 216
[49] Zhang J, Zhao D, Ma X and Yang J 2019 *J. Mol. Spectrosc.* **360** 7
[50] Zhang J, Zhao D, Xiang Q, Ma X and Yang J 2019 *J. Mol. Spectrosc.* **355** 96
[51] Zhang L, Yu Y, Cheng R and Yang J 2022 *J. Mol. Spectrosc.* **390** 111716
[52] Fang F, Zhou W, Li Y, Qian D, Luo C, Zhao D, Ma X and Yang J 2021 *Rev. Sci. Instrum.* **92** 043103
[53] Herzberg G 1950 *Spectra of Diatomic Molecules* (New York: Van Nostrand)
[54] Lefebvre-Brion H and Field R W 2004 *The Spectra and Dynamics of Diatomic Molecules* (New York: Academic Press)
[55] Western C M 2017 *J. Quant. Spectrosc. Radiat. Transf.* **186** 221
[56] de Laeter J R, Böhlke J K, de Bièvre P, Hidaka H, Peiser H S, Rosman K J R and Taylor P D P 2003 *Pure Appl. Chem.* **75** 683
[57] Halfen D T, Min J and Ziurys L M 2017 *J. Mol. Spectrosc.* **331** 1
[58] Mukund S, Yarlagadda S, Bhattacharyya S and Nakhate S G 2012 *J. Quant. Spectrosc. Radiat. Transf.* **113** 2004
[59] Breier A A, Waßmuth B, Fuchs G W, Gauss J and Giesen T F 2019 *J. Mol. Spectrosc.* **355** 46
[60] Gustavsson T, Amiot C and Vergès J 1991 *J. Mol. Spectrosc.* **145** 56
[61] Hocking W H, Gerry M C L and Merer A J 1979 *Can. J. Phys.* **57** 54
[62] Cheung A S C, Taylor A W and Merer A J 1982 *J. Mol. Spectrosc.* **92** 391
[63] Ishida M, Yamashiro R, Matsumoto Y and Honma K 2006 *J. Chem. Phys.* **124** 204316
[64] Gordon R M and Merer A J 1980 *Can. J. Phys.* **58** 642
[65] Cheung A S C, Gordon R M and Merer A J 1981 *J. Mol. Spectrosc.* **87** 289
[66] Clouthier D J, Huang G, Merer A J and Friedman-Hill E J 1993 *J. Chem. Phys.* **99** 6336
[67] Srdanov V I and Harris D O 1988 *J. Chem. Phys.* **89** 2748
[68] Ram R S and Bernath P F 1992 *J. Mol. Spectrosc.* **155** 315
[69] Appelblad O and Lagerqvist A 1975 *Can. J. Phys.* **53** 2221
[70] Appelblad O and Lagerqvist A 1973 *J. Mol. Spectrosc.* **48** 607
[71] Zack L N, Pulliam R L and Ziurys L M 2009 *J. Mol. Spectrosc.* **256** 186
[72] Moravec V D, Klopcic S A, Chatterjee B and Jarrold C C 2001 *Chem. Phys. Lett.* **341** 313
[73] Smirnov A N, Solomonik V G, Yurchenko S N and Tennyson J 2019 *Phys. Chem. Chem. Phys.* **21** 22794
[74] Bernard A, Bacis R and Luc P 1979 *Astrophys. J.* **227** 338
[75] Hoeft J and Törring T 1993 *Chem. Phys. Lett.* **215** 367
[76] Phillips J G and Davis S P 1976 *Astrophys. J. Suppl.* **32** 537
[77] Femenias J L and Cheval G 1987 *J. Mol. Spectrosc.* **124** 348
[78] Adam A G, Azuma Y, Barry J A, Merer A J, Sassenberg U, Schröder J O, Cheval G and Féménias J L 1994 *J. Chem. Phys.* **100** 6240
[79] Gertner M R, Shin J B and Nicholls R W 1993 *Spectrosc. Lett.* **26** 677
[80] Song P, Guan W, Yao C, Su M Z, Wu Z J, Feng J D and Yan L K 2007 *Theor. Chem. Acc.* **117** 407
[81] Wang N, Ng Y W and Cheung A S C 2013 *J. Phys. Chem. A* **117** 13279
[82] Yu Y, Zhang L, Niu Y, Zou W, Cheng R and Yang J 2022 *J. Quant. Spectrosc. Radiat. Transf.* **288** 108247
[83] Gengler J, Ma T, Adam A G and Steimle T C 2007 *J. Chem. Phys.* **126** 134304

[84] Jensen R H, Fougère S G and Balfour W J 2003 *Chem. Phys. Lett.* **370** 106

[85] Ramond T M, Davico G E, Hellberg F, Svedberg F, Salén P, Söderqvist P and Lineberger W C 2002 *J. Mol. Spectrosc.* **216** 1

[86] Almeida N M S, Ariyarathna I R and Miliordos E 2018 *Phys. Chem. Chem. Phys.* **20** 14578

[87] O'Brien L C, Wall S J and Sieber M K 1997 *J. Mol. Spectrosc.* **183** 1

[88] Bojović V, Antić-Jovanović A, Stoiljkoviać M M, Miletić M and Peĉić D S 1999 *Spectrosc. Lett.* **32** 875

[89] Chertihin G V and Andrews L 1997 *J. Chem. Phys.* **106** 3457

[90] Peterson K A, Shepler B C and Singleton J M 2007 *Mol. Phys.* **105** 1139

[91] Green D W 1971 *Can. J. Phys.* **49** 2552

[92] Green D W 1971 *J. Mol. Spectrosc.* **40** 501

[93] Hansson A, Pettersson A, Royen P and Sassenberg U 2004 *J. Mol. Spectrosc.* **224** 157

[94] Al-Khalili A, Hällsten U and Launila O 1999 *J. Mol. Spectrosc.* **198** 230

[95] Tovar K A and Varberg T D 2022 *J. Mol. Spectrosc.* **387** 111666

[96] Roberts M A, Alfonzo C G, Manke K J, Ames W M, Ron D B and Varberg T D 2007 *Mol. Phys.* **105** 917

[97] Balfour W and Ram R S 1984 *Can. J. Phys.* **62** 1524

[98] Yao C, Guan W, Song P, Su Z M, Feng J D, Yan L K and Wu Z J 2007 *Theor. Chem. Acc.* **117** 115

[99] Balfour W J and Ram R S 1984 *J. Mol. Spectrosc.* **105** 360

[100] Pang H F, Ng Y W and Cheung A S C 2012 *J. Phys. Chem. A* **116** 9739

[101] Sassenberg U and Scullman R 1977 *J. Mol. Spectrosc.* **68** 331

[102] Okabayashi T, Yamazaki E and Tanimoto M 2005 *J. Mol. Spectrosc.* **229** 283

[103] Sassenberg U and Scullman R 1983 *Physica Scripta* **28** 139

[104] O'Brien L C, Hardimon S C and O'Brien J J 2004 *J. Phys. Chem. A* **108** 11302

[105] Xiang Q L, Yang J, Zhang S L, Zhang J C and Ma X W 2019 *Spectrosc. Lett.* **52** 21

[106] Okabayashi T, Koto F, Tsukamoto K, Yamazaki E and Tanimoto M 2005 *Chem. Phys. Lett.* **403** 223

[107] Chambaud G, Guitou M and Hayashi S 2008 *Chem. Phys.* **352** 147

[108] Schwerdtfeger P, Dolg M, Schwarz W H E, Bowmaker G A and Boyd P D W 1989 *J. Chem. Phys.* **91** 1762